ck for updates

ChemPubSoc Europe

DOI: 10.1002/cphc.201800382

CHEMPHYSCHEM Articles

Density Functional Theory – Machine Learning Approach to Analyze the Bandgap of Elemental Halide Perovskites and Ruddlesden-Popper Phases

Omar Allam[+,[a, b]] Colin Holmes[+,[a]] Zev Greenberg,[[a]] Ki Chul Kim,[[a, c]] and Seung Soon Jang*[[a, d, e, f]]

In this study, we have developed a protocol for exploring the vast chemical space of possible perovskites and screening promising candidates. Furthermore, we examined the factors that affect the band gap energies of perovskites. The Goldschmidt tolerance factor and octahedral factor, which range from 0.98 to 1 and from 0.45 to 0.7, respectively, are used to filter only highly cubic perovskites that are stable at room temperature. After removing rare or radioactively unstable elements, quantum mechanical density functional theory calculations are performed on the remaining perovskites to assess whether their electronic properties such as band structure are suitable for solar cell applications. Similar calculations are performed on the Ruddlesden-Popper phase. Furthermore, machine learning was utilized to assess the significance of input parameters affecting the band gap of the perovskites.

1. Introduction

As fossil fuel resources become increasingly depleted, it is quintessential that alternative sustainable sources of energy have been rigorously investigated. Hence, it is very desirable to widen the spectrum of energy resources available given increasing demand of energy in modern civilization. Among various energy resources, photovoltaic technology is one of the most promising candidates providing consistent and steady source of electrical energy.

It should be noted, however, that silicon, the most prominently used material in photovoltaic technology, involves a manufacturing process requiring very high temperature conditions, which yields high manufacturing costs.[1] Additionally, silicon photovoltaic cells have poor flexibility against its mechanical deformation, which imposes significant limitation on practical applications. As such, it is critical to find alternative solar cell materials that have better efficiency and flexibility as well as less manufacturing costs.[2]

In this context, perovskite has attracted lots of attention as a promising material for solar cell technology due to its high solar conversion efficiency.[3] For instance, the optimal band gap of a photovoltaic (~1.34 eV) adheres to the Shockley-Queisser Limit with a solar conversion efficiency of 33.5%,[3] whereas the most popular solar cell material, silicon, has a less desirable band gap of 1.1 eV with the maximum theoretical conversion efficiency to 32%.[1,4] However, it has been noted that the perovskite has notorious structural instability with respect to moisture and electric field. Since it is challenging to find a solar cell material that has both high stability with the optimal band gap, a great deal of efforts has been dedicated to develop new materials with improved stability and band structure. For instance, Ruddlesden-Popper phase[3,5] has been discovered to be stable with respect to UV and humidity.[4,6]

Stoumpos and his coworkers[5c] have reported how the ratio between the spacer cation and the small organic cation, so-called n-factor, can influence the band gap and the efficiency of the perovskites, showing a negative proportionality between the n-factor and the band gap for 2D hybrid lead iodide perovskites.[5c] Inspired by their study, in this study, we investigate the tunability of the band gap of elemental perovskite crystals using quantum mechanical density functional theory (DFT) and machine learning (ML), and thereby elucidate how we can use the n-factor in Ruddlesden-Popper phase in order to tune the band gap. Further, we investigate how the band-gap is correlated with the n-factor when it comes to 2D elemental halide perovskites. Then, finally, we attempt to form a screening strategy to obtain structurally stable layered perovskites.

In our computations, all possible elemental perovskites with the composition of ABX_3 are examined for screening based on the criteria of geometrical stability of elemental perovskite,

[a] O. Allam,[+] C. Holmes,[+] Z. Greenberg, Prof. K. C. Kim, Prof. S. S. Jang
Computational NanoBio Technology Laboratory, School of Materials Science and Engineering, Georgia Institute of Technology, Atlanta, GA 30332-0245, USA
E-mail: SeungSoon.Jang@mse.gatech.edu
[b] O. Allam[+]
The George W. Woodruff School of Mechanical Engineering, Georgia Institute of Technology, Atlanta, GA 30332-0405, USA
[c] Prof. K. C. Kim
Department of Chemical Engineering, Konkuk University, Seoul 05029, Republic of Korea
[d] Prof. S. S. Jang
Institute for Electronics and Nanotechnology, Georgia Institute of Technology, Atlanta, GA 30332, USA
[e] Prof. S. S. Jang
Parker H. Petit Institute for Bioengineering and Bioscience, Georgia Institute of Technology, Atlanta, GA 30332, USA
[f] Prof. S. S. Jang
Strategic Energy Institute, Georgia Institute of Technology, Atlanta, GA, 30332, USA
[+] These authors contributed equally to this work.

© 2018 Wiley-VCH Verlag GmbH & Co. KGaA, Weinheim

14397641, 2018, 19, Downloaded from https://chemistry-europe.onlinelibrary.wiley.com/doi/10.1002/cphc.201800382 by ITMO University, Wiley Online Library on [12/11/2025]. See the Terms and Conditions (https://onlinelibrary.wiley.com/terms-and-conditions) on Wiley Online Library for rules of use; OA articles are governed by the applicable Creative Commons License

such as Goldschmidt tolerance and octahedral factor.[7] Then, DFT calculations are performed to in order to obtain the band gap.

Advanced quantum mechanical DFT modeling offers a great opportunity for the materials science community to characterize the electronic, structural, thermodynamic, and mechanical properties of thousands of materials, especially when combined with high-throughput screening techniques.[7a,b,8] As such, intensive investigations of the immense chemical spectrum are being increasingly pursued, which enables scientists to design and discover new photovoltaic materials with optimal properties.[7a]

In this context, machine learning (ML) would also be utilized with DFT for high-throughput screening of new materials. ML is one of artificial intelligence algorithms that can achieve its predictive capability by learning from data.[9] Through recent reports, it has been demonstrated that ML can be used in materials science in order to predict complex behaviors of materials and thereby to help explore vast chemical space for new materials discovery.[7a,b,9] For instance, once a machine learning algorithm is properly trained, it may provide the immediate prediction of electrical properties of materials, which otherwise would have taken significantly longer time to obtain results from experiments or other computations such as DFT.

In this investigation, we employ DFT and ML to analyze how basic atomic information such as ionic radii and charges can be used as input data affect the band gaps of inorganic layered and non-layered perovskites.

2. Results and Discussion

2.1. Layered Perovskites

Perovskite can be represented as a cage-like structure in which A represent a large cation at the corners while B is the smaller cation at the center, forming the face-centered bipyramidal portion with X, as shown in Figure 1 by Perovskite 1 and 2. It is the large space inside the perovskite structure, relative to the X anion, which is likely responsible for some electronic properties of perovskites such as piezoelectricity, pyroelectricity, and photovoltaics. The basic perovskite formula ABX_3 was used in developing possible elemental-halide combinations from periodic table, which conforms to the stoichiometry.

Furthermore, the Goldschmidt tolerance factor was used in order to filter the perovskite combinations for cubic perovskite, whose value was ranged from 0.98 to 1.00,[10] which is helpful to predict the crystal lattice structure of perovskites. Cubic perovskites are of interest in this case because cubic perovskites tend to be more stable in Ruddlesden-Popper phase, which is the desired end structure for this investigation. Approximately 220 ABX_3 halide perovskites were found to the Goldschmidt tolerance factor of 0.98–1.00. Furthermore, another investigation has shown that a certain data set of ABX_3 halide perovskites with high formability has the octahedral factor, the ratio of r_B to r_A, between approximately 0.45 and 0.70.[7b] Therefore, in addition to a narrow Goldshcmidt Tolerance factor ranging from 0.98 to 1.00 for the high probability of being cubic, the perovskites were filtered using the octahedral factor of 0.45–0.70.

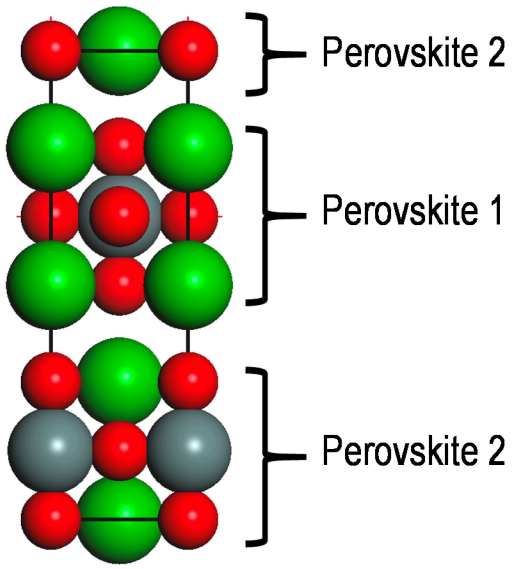

Figure 1. Atomic structure of single layered barium stanate ($BaSnO_3$ – Ruddlesden-Popper phase). Green, red, and gray colors denote Ba, O, and Sn.

Next, after the removal of most radioactive elements compositions, the base data set was eventually downsized to 14 perovskites. Out of the 14 candidates, 9 candidates were stable after geometrically optimization and proceeded to the next stage of the study. The candidates are composed of Am, Au, Ba, Cs, K and Pd for the A site, Ba, Mn, Fe, Cu, V, Sn, Cr, and Se for the B site, and Cl, Fl, and O for the X site. The majority of perovskites in this space were found to have relatively low band gap ranging from approximately 0.158 eV to 0.677 eV, as seen in Figure 2a. The two exceptions in this case were potassium iron fluoride ($KFeF_3$) and barium stanate ($BaSnO_3$) with band gaps of 1.734 eV and 2.786 eV, respectively. In addition to the 14 perovskite candidates obtained using the filtering method mentioned above, seven additional perovskites of particular interest in past investigations have been examined computationally.[7c,11] These perovskites were potassium metal fluorides (KMF_3, were M = Zn, Ni, Co, and Cu),[11] and cesium metal halides ($CsMX_3$, were M = Pb and Sn, and X = Cl, Br, and I).[7c] The majority of the potassium metal fluorides were observed to have relatively small band gaps ranging from 0.0627 eV to 0.338 eV, with the exception of potassium zinc fluoride whose band gap was computationally predicted to be 4.024 eV. On the other hand, a majority of the cesium metal halides were observed to have relatively large band gaps ranging from 1.951 eV to 2.575 eV, with the exception of cesium copper chloride with the bandgap of 0.403 eV. Thus, a group of 16 perovskites proceeded to the next stage of the study which was to investigate their layered phase (Ruddlesden-Popper). A total of 56 cases which included 3D and 2D perovskites were investigated in this study for their band gaps.

© 2018 Wiley-VCH Verlag GmbH & Co. KGaA, Weinheim

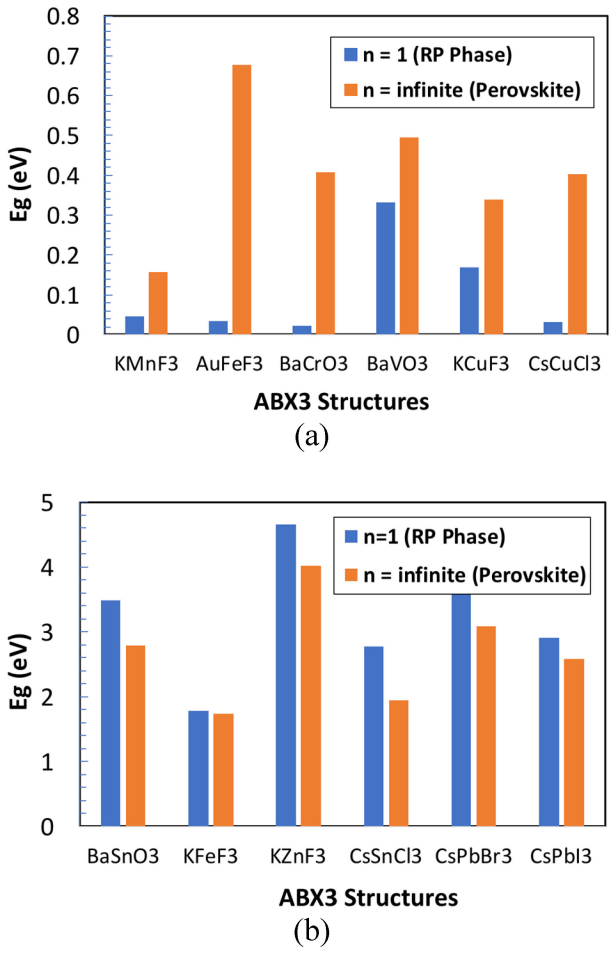

Figure 2. (a) Band gap of single layered Ruddlesden-Popper phase structure (blue bars) and perovskite phase structure (orange bars) for low bandgap ABX_3 crystals; (b) band gap of single layered Ruddlesden-Popper Phase structure and perovskite phase structure for high band gap ABX_3 crystals.

2.2. Ruddlesden-Popper (RP) Phase

Layered perovskites (RP phased perovskites, as seen in Figure 1) have recently drawn attention as possible stable alternatives to non-layered perovskites.[5a,c,12] However, the solar conversion efficiency of the RP Phased perovskites of ~4.73%[3] needs to be improved for practical applications. In this study, it is attempted to investigate the effect of the number of perovskite layers between each inorganic rock-salt layer on the band gap of the RP phase.

First, the single layered RP phase structure (n = 1) is studied. The perovskites were divided into two groups (low band gap and high band gap perovskites) using the threshold value of 0.7 eV. As seen in Figure 2a, a majority of the low band gap perovskites have larger band gaps in their non-layered phase compared to their layered phase (RP phase): the increase of band gap is observed in the range from 49% for barium vanadium oxide ($BaVO_3$) to 1854% for gold iron fluoride ($AuFeF_3$). The exceptions to this trend are potassium nickel fluoride ($KNiF_3$) and potassium cobalt fluoride ($KCoF_3$), whose non-layerd phases show smaller band gap by 76% and 37%, respectively, compared to the RP phase.

On the other hand, the RP phases of high band gap perovskites ($E_g > 0.7$ eV) show an opposite trend in comparison to low band gap perovskites ($E_g < 0.7$ eV).[5c] First, it is found in Figure 2b that the differences in band gaps between the layered and non-layered structures for high band gap perovskites were significantly less than those for low band gap perovskites. Furthermore, the non-layered perovskite phase was always calculated to have a lower band gap than the layered perovskite phase (Ruddlesden-Popper phase), ranging from 3% decrease for potassium iron fluoride to a 30% decrease for cesium tin chloride.

This substantial difference in the band gap between layered and non-layered perovskites provides the possibility of tuning the band gap of the perovskite in order to optimize its solar conversion efficiency by altering the number of layers between each rock-salt layer. We hypothesized that the most logical outcome would be that the band gap of the layered perovskite (n = 1) would approach that of the non-layered perovskite (n = ∞), as the number of layered slabs is increased.[5c] It was theorized that the band gap would increase for the low band gap perovskites and decrease for the high band gap perovskites, by increasing the number of layered perovskites.

As such, DFT calculations were performed for n = 2, n = 3, n = 4, and n = 5 for nearly 14 layered perovskite structures to obtain their band gaps.[5c] It is observed in Figure 3a that the low band gap perovskites typically show fluctuating band gaps with increasing the number of layers. For instance, cesium copper chloride shows band gaps of 0.0328 eV, 0.295 eV, 0.0195 eV, 0.156 eV, 0.0450 eV, and 0.402 eV for n = 1, 2, 3, 4, 5, and ∞, respectively. On the other hand, as shown in Figure 3b, the high band gap perovskites show monotonous behavior towards the non-layered perovskite band gap with increasing the number of layers, as is hypothesized.[5c] The only exception to this trend was the potassium iron fluoride whose band gap decreases below the value of the non-layered phase band gap ranging from n = 3 to n = 5.

2.3 Machine Learning Approach

To further understand our DFT results, the artificial neural network method is used. Although artificial neural network is a useful predictive tool, the main purpose for its use in this investigation is to correlate various factors with the band gap and analyze the importance of such factors.[9] The input parameters of the artificial neural network are the following: 1) the inverse of the number of layers between rock salt layers;[5c] 2) the ionic radii of A, B, and X; 3) the oxidation states of A, B, and X. Provided each of these inputs, a specific perovskite can be surmised. The output of the artificial neural network is the band gap (varied between direct and indirect) of each layered/non-layered perovskite, which is obtained computationally. 56 cases are used in the artificial neural network, out of which 60% are used for training the algorithm, 20% are used as testing instances, and another 20% are used as selection

© 2018 Wiley-VCH Verlag GmbH & Co. KGaA, Weinheim

14397641, 2018, 19, Downloaded from https://chemistry-europe.onlinelibrary.wiley.com/doi/10.1002/cphc.201800382 by ITMO University, Wiley Online Library on [12/11/2025]. See the Terms and Conditions (https://onlinelibrary.wiley.com/terms-and-conditions) on Wiley Online Library for rules of use; OA articles are governed by the applicable Creative Commons License

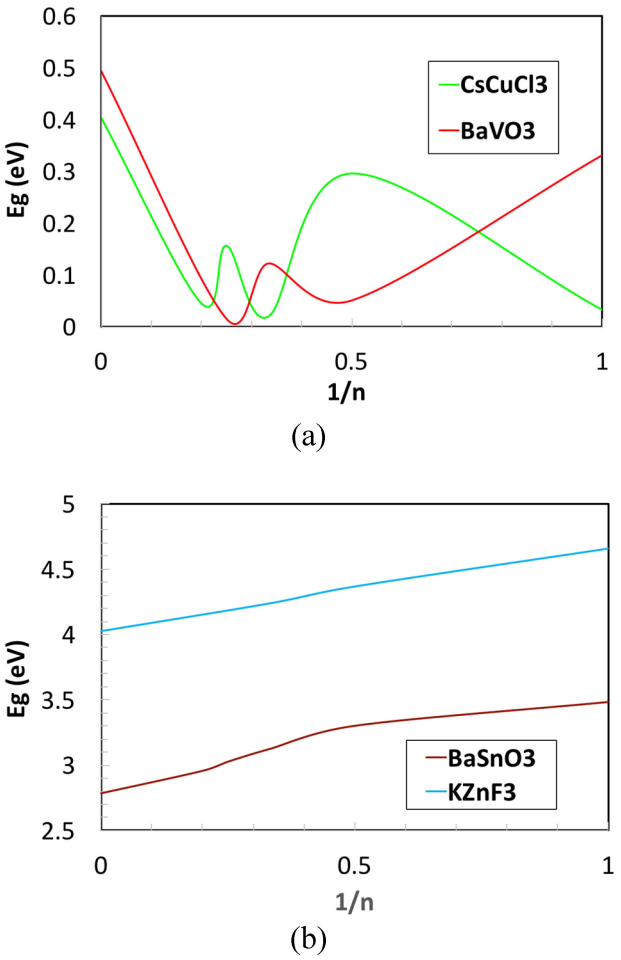

Figure 3. Effect of the number of perovskite layers between rock-salt layers on the band gap of ABX_3 Ruddlesden-Popper Phase for both the low and high band gap cases: (a) the band gap variation for low band gap $CsCuCl_3$ and $BaVO_3$ RP structures; (b) the band gap variation for high bandgap $BaSnO_3$ and $KZnF_3$ RP structures.

instances (to choose the model with the best generalization properties).[13]

As shown in Figure 4a, a linear regression analysis demonstrates that the artificial neural network provides very accurate band gap prediction, which is in good greement with the DFT results. Table 1 displays the agreement of the band gap prediction between the artificial neural network and DFT with the average error of ~3%. It seems that this is quite promising given the relatively limited amount of input data.

Table 1. Comparison between the DFT and machine learning predicted bandgaps of five ABX_3 RP structures with various number of layers that are not included in the original machine learning data set.

Structure	Band gap [eV] (DFT)	Band gap [eV] (Artificial Neural Network)	error [%]
$kcuf_3$ (n = 2)	0.197	0.208	5.580
$cssnCl_3$ (n = 1)	2.774	2.770	0.144
$cspbl_3$ (n = 1)	2.907	2.957	1.690
$cspbbr_3$ (n = 1)	3.571	3.867	8.290
$basno_3$ (n = 3)	3.127	3.118	0.288

Table 2. The input parameters used by the machine learning to produce various cuts of the neural network model, in which the correlation of each input with the output was examined whilst keeping the rest of the inputs constant. The following data set is the case of 3D $KFeF_3$ perovskite.

Inputs	Values
1/n	0
ra (pm)	152
rb (pm)	75
rx (pm)	119
ca (e)	1
cb (e)	2
cx (e)	−1

The individual contributions of the input variables are also analyzed in order to evaluate their importance in affecting the band gap. If a contribution factor of an input variable is less than 1, it means that removing the input variable decreases the error of the neural network, and vice versa. Figure 4b shows that all the inputs are well over 1, indicating that all the input variables are significantly important in determining the band gap. The most noteworthy point found in Figure 4b is that the number of layers between rock salt phases is the most influencing input variable, followed closely by the oxidation state of the X anion and the ionic radius of the A cation.

It would be very insightful if we can see how the band gap (output) varies as a function of a single input parameter while the rest are fixed. Essentially, this 'directional output' is a cut of the neural network model along a certain input direction and a certain reference point.[13] Although the directional output may vary depending on the reference point, it can still be useful as it can provide an overall basis regarding the correlation between the inputs and the output. The input values shown in Table 2 for the case of 3D $KFeF_3$ perovskite produce the directional outputs for the radii of the A and B, shown in Figures 4c and 4d. The band gap and the radius of A show a very positive correlation between 149.3 pm until 162.01 pm, but beyond this range, the band gap is not significantly influenced by the radius of the A cation. This high correlation within the mentioned range can be seen in Table 3, where the DFT band gap is increased from 0.624 eV to 1.73 eV by changing the radius of A cation from 151 pm to 152 pm, while keeping all other inputs constant (going from $AuFeF_3$ to $KFeF_3$). As such, a slight change in the radius of the A cation in the region between 149.3 pm and 162.01 pm may result in significant changes in the band gap. Furthermore, as seen in Figure 4d, the band gap and the radius of the B cation are very negatively correlated between

Table 3. Change in band gap obtained by rA manipulation.

Parameters	Values ($AuFeF_3$)	Values ($KFeF_3$)
1/n	0	0
ra (pm)	151	152
rb (pm)	75	75
rx (pm)	119	119
ca (e)	1	1
cb (e)	2	2
cx (e)	−1	−1
Eg (eV)	0.624	1.732

© 2018 Wiley-VCH Verlag GmbH & Co. KGaA, Weinheim

14397641, 2018, 19, Downloaded from https://chemistry-europe.onlinelibrary.wiley.com/doi/10.1002/cphc.201800382 by ITMO University, Wiley Online Library on [12/11/2025]. See the Terms and Conditions (https://onlinelibrary.wiley.com/terms-and-conditions) on Wiley Online Library for rules of use; OA articles are governed by the applicable Creative Commons License

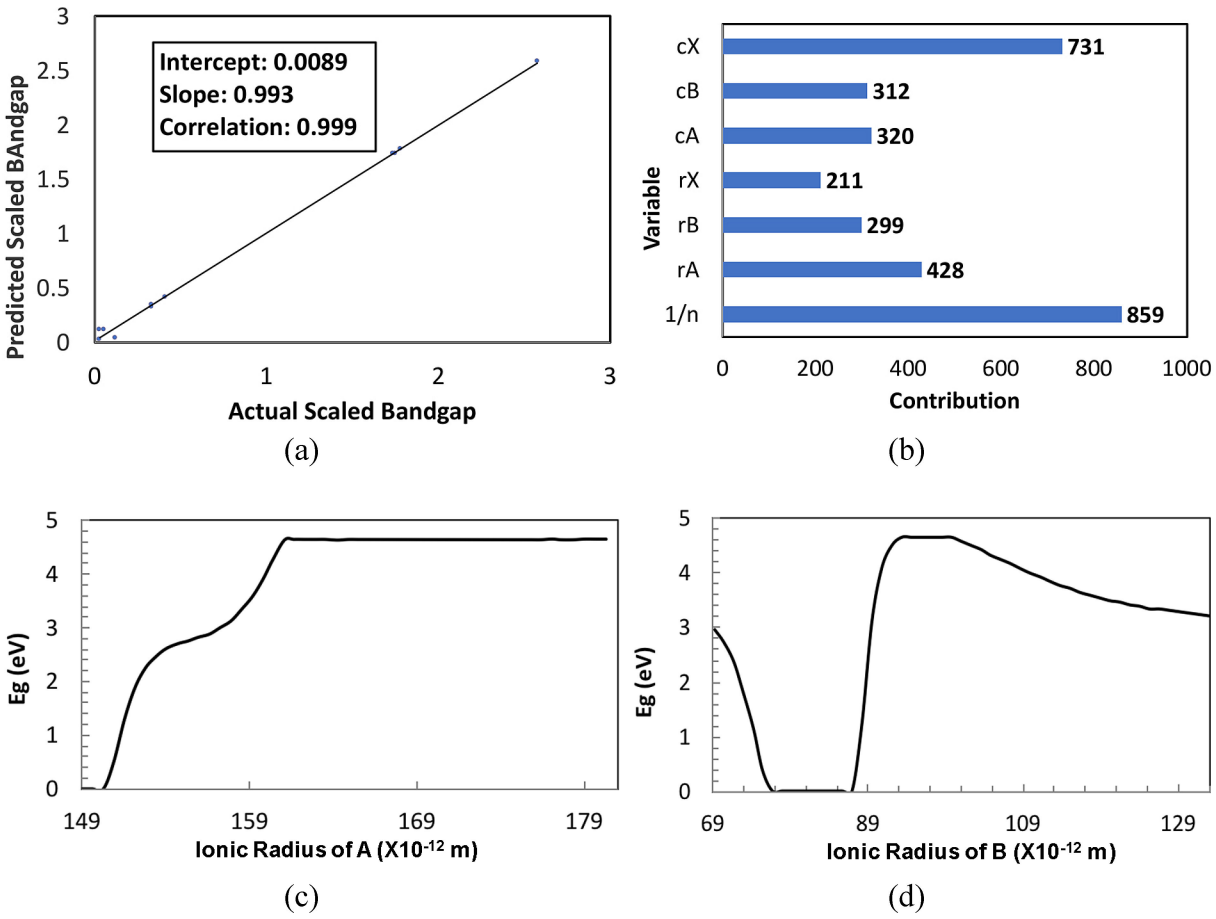

Figure 4. (a) The correlation of the band gaps predicted by machine learning with the DFT predicted band gaps; (b) the contributions of each input variable to the band gaps in the machine learning; (c) the correlation between the output band gap and the ionic radius of A, keeping all other input variables constant; (d) the correlation between the output band gap and the ionic radius of B, keeping all other input variables constant.

nearly 69.23 pm and 76.66 pm, and very highly correlated between 86.92 pm and 94.62 pm.

Despite encompassing a limited range of data, this study demonstrates that the artificial neural network can be used to accurately predict the band gap of undiscovered perovskites within the range of input cases. It is important to note that the band gap values predicted via machine learning will be agreed with DFT-based band gap using PBE functional. As such, in order to derive band gaps that align with experimental data, it is suggested to train the artificial neural network using band gaps obtained from more computationally expensive and robust methods such as HSE06.[7c,14]

3. Conclusions

A high throughput screening method has been applied in order to search for ABX_3 inorganic two-dimensional perovskites with a high probability of stability for both the non-layered phases and the layered Ruddlesden-Popper phases. The series in this study included various number of layers ($n=1$, 2, 3, 4, 5, and ∞). Using DFT method, first, the structural relaxations were performed, and then the band gap energies were obtained. The effects of various factors such as ionic radii and oxidation states of A, B, and X had on the DFT band gap were examined. The structures were divided into groups of perovskite: low band gap group ($E_g < 0.7$ eV) and high band gap ($E_g > 0.7$ eV). First, it was observed that the low band gap perovskites exhibited an overall trend in which the perovskite phase had a higher band gap than the Ruddlesden-Popper phase with $n=1$, while the the rest of the low band gap group ($n=2$, 3, 4, and 5) exhibited an oscillatory behavior between the cases with $n=1$ and ∞.

On the other hand, the high band gap group exhibited that the first layered perovskite series ($n=1$) always had a larger band gap energy than the non-layered series. In general, it was observed that the band gap gradually approached that of the non-layered perovskite as the number of layer is increased. The only exception to this was for potassium iron fluoride, whose band gap energy for $n=3,4$, and 5 was decreased to have samller band gap than that of the non-layered series ($n=\infty$). However, it is still possible that the band gap rebounds again as the number of layers approaches infinity.

Lastly, the machine learning was used to analyze the importance of input parameters with respect to the band gap energy. It was found that the number of layer of perovskite

© 2018 Wiley-VCH Verlag GmbH & Co. KGaA, Weinheim

14397641, 2018, 19, Downloaded from https://chemistry-europe.onlinelibrary.wiley.com/doi/10.1002/cphc.201800382 by ITMO University, Wiley Online Library on [12/11/2025]. See the Terms and Conditions (https://onlinelibrary.wiley.com/terms-and-conditions) on Wiley Online Library for rules of use; OA articles are governed by the applicable Creative Commons License

between rock salt phases (n), the oxidation state of the anion forming the external octahedral *cage* (X), and the ionic radii of the cations forming the rest of the extenal cage were the most important factors that affected the band gap.

In this study, therefore, it is clearly demonstrated that the new perovskite materials could be designed using DFT and machine learning in addition to experimental approach.

3.1. Computational Methods

3.1.1. Density Functional Theory Approach

Density functional theory (DFT) calculations have been widely used in order to analyze the electronic properties, particularly the band structure of materials such as semiconductors in general. In this study, therefore, we employed DFT via the Cambridge Serial Total Energy Package (CASTEP)[15] package in Materials Studio.[16] The structures of inorganic ABX_3 perovskites were optimized using Broyden-Fletcher-Goldfarb-Shanno algorithm[17] in order to characterize the band structures and find the ground-state energy. The General Gradient Approximation (GGA) Perdew-Burke-Ernzerhof (PBE) functional was used.[18]

It has been well known that GGA PBE may often grossly underestimate the band gap of perovskites in general as observed with $CsCuCl_3$[19] in this investigation despite a few exceptions predicting band gaps accurately for certain perovskites such as $BaSnO_3$.[19–20] Thus, HSE is often recommended in order to obtain reliable band gap energies that align more closely with experimental results.[7c,14] However, it should be noted that a great deal of results using GGA PBE fell within a reasonable range of values consistently, and, in fact, the effects of altering A, B, and X on the change of band gap are similarly observed as in another computational study using HSE accounting for spin-orbit coupling effect.[7c] Another noteworthy point is that GGA PBE is very efficient and fast for studying a relatively large size of layered perovskites as examined in this study,[21] which is critically important in our high-throughput screen application for filtering perovskites. Thus, it is assumed that we can still make a reasonable conclusion by taking into account the underestimation of band gap from GGA PBE.

On the other hand, the Goldschmidt Tolerance Factor is used in order to filter the perovskite spectrum for cubic crystals to a certain degree of tolerance which is allowed for perovskites.[10] The ionic radii of the A, B and X ions are utilized to estimate the parameter of the cell and the coordinates of the ions. The approximated lattice parameters of perovskite crystal were obtained by the following definitions:

$$a = b = c = \sqrt{2}(r_A + r_B)$$

The approximated crystal lattice parameters of Ruddlesden-Popper phase were obtained by the following definitions:

$$a = c = \sqrt{2} \cdot (r_A + r_B)$$

$$b = 2 \cdot a \cdot n + \sqrt{2} \cdot a$$

To determine the probable perovskite crystalline structures with reasonable lattice parameters, the BFGS minimization algorithm in CASTEP was performed with cell optimization, which uses Hessian matrix that is updated during the iterative process until the energy minimization is converged.[17] Then, the band structure was calculated for the geometrically optimized structures.

The self-consistent field (SCF) convergence tolerance was 1×10^{-6} eV/atom with a smearing of 0.3 eV, and the k-point sampling of $6 \times 1 \times 6$, $6 \times 2 \times 6$, and $6 \times 6 \times 6$.[22] The Ruddlesden-Popper structures were prepared with n = 1, 2, 5, and ∞ phases.[5d] The reciprocal space was representated along with norm-conserving method to handle electron ion interactrions for the calculations.

3.2. Machine Learning Approach

In this study, the Quasi-Newton method was used as the training algorithm for the artificial neural network.[23] The Quasi-Newton method are arguably one of the most popular numerical optimization methods, which are used in a wide range of numerical applications including machine learning. Compared to the Newton's method that requires the calculation of the Hessian matrix consisting of the second partial derivative of the loss function,[23] the Quasi-Newton method estimates the inverse Hessian matrix at each iteration using only the first partial derivative of the loss function without calculating the exact value of Hessian, which makes this method less expensive.[23] For this purpose, the Normalized Squared Error function was used in Neural Designer[13] with a maximum iteration of 5000. As presented in Figure 5, two

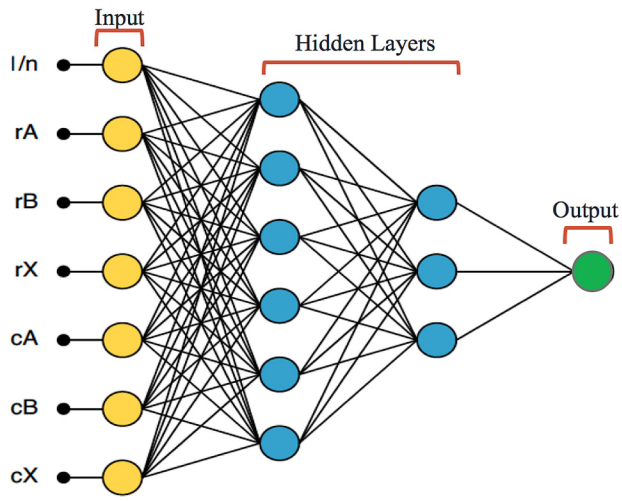

Figure 5. Artificial neural network with seven inputs and two hidden layers.

© 2018 Wiley-VCH Verlag GmbH & Co. KGaA, Weinheim

14397641, 2018, 19, Downloaded from https://chemistry-europe.onlinelibrary.wiley.com/doi/10.1002/cphc.201800382 by ITMO University, Wiley Online Library on [12/11/2025]. See the Terms and Conditions (https://onlinelibrary.wiley.com/terms-and-conditions) on Wiley Online Library for rules of use; OA articles are governed by the applicable Creative Commons License

hidden layers were used with six and three nodes in the first and second layer, respectively. It was determined that more hidden layers were unnecessary given the relatively small number of cases (56 cases) that were fed to our neural network, and additionally, a very satisfactory stage was reached, demonstrating an average error of 3.19% in predicting band gaps outside the original cases.

ANN was deemed suitable for our study as it possessed the ability of implicitly classifying complex nonlinear relationships between a relatively large number of variables. Even though one of the main disadvantages of ANN is that it can be computationally burdensome, this was not a major issue in this study due to the relative size of the dataset. Although ANN has a well-established forecasting capability, it was primarily used in this study for its regressive or interpolative capability to investigate the characteristics that influence band gap.

Acknowledgement

We acknowledge that Omar Allam was supported by President Undergraduate Research Award (PURA) of Georgia Institute of Technology.

Conflict of Interest

The authors declare no conflict of interest.

Keywords: Perovskite · Ruddlesden-Popper phase · Density Functional Theory · Machine Learning · High-Throughput Screening

[1] Z. Song, C. L. McElvany, A. B. Phillips, I. Celik, P. W. Krantz, S. C. Watthage, G. K. Liyanage, D. Apul, M. J. Heben, *Energy Environ. Sci.* **2017**, *10*, 1297–1305.
[2] H. J. Snaith, *J. Phys. Chem. Lett.* **2013**, *4*, 3623–3630.
[3] H. H. Tsai, W. Y. Nie, J. C. Blancon, C. C. S. Toumpos, R. Asadpour, B. Harutyunyan, A. J. Neukirch, R. Verduzco, J. J. Crochet, S. Tretiak, L. Pedesseau, J. Even, M. A. Alam, G. Gupta, J. Lou, P. M. Ajayan, M. J. Bedzyk, M. G. Kanatzidis, A. D. Mohite, *Nat.* **2016**, *536*, 312–316.
[4] J. E. Parrott, Theoretical upper limit to the conversion efficiency of solar energy, Vol. 21, **1978**.
[5] a) Y. Yu, D. D. Zhang, P. D. Yang, *Nano Lett.* **2017**, *17*, 5489–5494; b) T. M. Koh, B. Febriansyah, N. Mathews, *Chem* **2017**, *2*, 326–327; c) C. C. Stoumpos, C. M. M. Soe, H. Tsai, W. Y. Nie, J. C. Blancon, D. Y. H. Cao, F. Z. Liu, B. Traore, C. Katan, J. Even, A. D. Mohite, M. G. Kanatzidis, *Chem* **2017**, *2*, 427–440; d) C. C. Stoumpos, D. H. Cao, D. J. Clark, J. Young, J. M. Rondinelli, J. I. Jang, J. T. Hupp, M. G. Kanatzidis, *Chem. Mater.* **2016**, *28*, 2852–2867.
[6] a) D. Wang, M. Wright, N. K. Elumalai, A. Uddin, *Sol. Energy Mater. Sol. Cells* **2016**, *147*, 255–275; b) J. B. You, L. Meng, T. B. Song, T. F. Guo, Y. Yang, W. H. Chang, Z. R. Hong, H. J. Chen, H. P. Zhou, Q. Chen, Y. S. Liu, N. De Marco, Y. Yang, *Nat. Nanotechnol.* **2016**, *11*, 75–81; c) M. Kaltenbrunner, G. Adam, E. D. Glowacki, M. Drack, R. Schwodiauer, L. Leonat, D. H. Apaydin, H. Groiss, M. C. Scharber, M. S. White, N. S. Sariciftci, S. Bauer, *Nat. Mater.* **2015**, *14*, 1032–1039; d) X. Li, M. I. Dar, C. Y. Yi, J. S. Luo, M. Tschumi, S. M. Zakeeruddin, M. K. Nazeeruddin, H. W. Han, M. Gratzel, *Nat. Chem.* **2015**, *7*, 703–711; e) D. H. Cao, C. C. Stoumpos, O. K. Farha, J. T. Hupp, M. G. Kanatzidis, *J. Am. Chem. Soc.* **2015**, *137*, 7843–7850; f) Y. Han, S. Meyer, Y. Dkhissi, K. Weber, J. M. Pringle, U. Bach, L. Spiccia, Y. B. Cheng, *J. Mater. Chem. A* **2015**, *3*, 8139–8147.
[7] a) C. Kim, G. Pilania, R. Ramprasad, *J. Phys. Chem. C* **2016**, *120*, 14575–14580; b) G. Pilania, P. V. Balachandran, C. Kim, T. Lookman, *Front. Mater.* **2016**, *3*; c) L. Lang, J.-H. Yang, H.-R. Liu, H. J. Xiang, X. G. Gong, *Phys. Lett. A* **2014**, *378*, 290-293.
[8] J. W. Lee, Y. T. Hsieh, N. De Marco, S. H. Bae, Q. F. Han, Y. Yang, *J. Phys. Chem. Lett.* **2017**, *8*, 1999–2011.
[9] T. Mueller, A. G. Kusne, R. Ramprasad, in *Reviews in Computational Chemistry, Vol 29, Vol. 29* (Eds.: A. L. Parrill, K. B. Lipkowitz), Wiley-Blackwell, Malden, **2016**, pp. 186–273.
[10] Z. Li, M. J. Yang, J. S. Park, S. H. Wei, J. J. Berry, K. Zhu, *Chem. Mater.* **2016**, *28*, 284–292.
[11] Hayatullah, G. Murtaza, R. Khenata, S. Muhammad, A. H. Reshak, K. M. Wong, S. Bin Omran, Z. A. Alahmed, *Comput. Mater. Sci.* **2014**, *85*, 402–408.
[12] a) A. H. H. Ramadan, L. Hesselmann, R. A. De Souza, *J. Phys. Chem. Solids* **2015**, *86*, 90–94; b) M. Lehtimaki, H. Yamauchi, M. Karppinen, *J. Solid State Chem.* **2013**, *204*, 95–101; c) J. Yu, J. Sunarso, Y. L. Zhu, X. M. Xu, R. Ran, W. Zhou, Z. P. Shao, *Chem. Eur. J.* **2016**, *22*, 2719–2727.
[13] Neural Designer, v. 2.90, Artelnics, **2018**.
[14] J. Lee, A. Seko, K. Shitara, K. Nakayama, I. Tanaka, *Phys. Rev. B* **2016**, *93*, 115104.
[15] S. J. Clark, M. D. Segall, C. J. Pickard, P. J. Hasnip, M. J. Probert, K. Refson, M. C. Payne, *Zeitschrift Fur Kristallographie* **2005**, *220*, 567–570.
[16] Materials Studio, v.5.0, Accelrys Software Inc., San Diego, **2007**.
[17] B. G. Pfrommer, M. Cote, S. G. Louie, M. L. Cohen, *J. Comp. Physiol.* **1997**, *131*, 233–240.
[18] J. P. Perdew, K. Burke, M. Ernzerhof, *Phys. Rev. Lett.* **1996**, *77*, 3865–3868.
[19] M. Aamir, M. Sher, M. A. Malik, J. Akhtar, N. Revaprasadu, *New J. Chem.* **2016**, *40*, 9719–9724.
[20] A. Prakash, P. Xu, A. Faghaninia, S. Shukla, J. W. Ager, C. S. Lo, B. Jalan, *Nat. Commun.* **2017**, *8*, 15167.
[21] A. Seidl, A. Gorling, P. Vogl, J. A. Majewski, M. Levy, *Phys. Rev. B* **1996**, *53*, 3764–3774.
[22] J. D. Pack, H. J. Monkhorst, *Phys. Rev. B* **1977**, *16*, 1748–1749.
[23] P. Hennig, M. Kiefel, *J. Mach. Learn. Res.* **2013**, *14*, 843–865.

Manuscript received: April 24, 2018
Accepted Article published: June 21, 2018
Version of record online: July 5, 2018

© 2018 Wiley-VCH Verlag GmbH & Co. KGaA, Weinheim

14397641, 2018, 19, Downloaded from https://chemistry-europe.onlinelibrary.wiley.com/doi/10.1002/cphc.201800382 by ITMO University, Wiley Online Library on [12/11/2025]. See the Terms and Conditions (https://onlinelibrary.wiley.com/terms-and-conditions) on Wiley Online Library for rules of use; OA articles are governed by the applicable Creative Commons License